Available online at www.sciencedirect.com
SCIENCE DIRECT®
Composites Science and Technology 66 (2006) 2423–2435
COMPOSITES SCIENCE AND TECHNOLOGY
www.elsevier.com/locate/compscitech

Facesheet delamination of composite sandwich materials at cryogenic temperatures

Thomas S. Gates [a,*], Xiaofeng Su [c], Frank Abdi [c], Gregory M. Odegard [b], Helen M. Herring [a]

[a] NASA Langley Research Center, Hampton, VA 23681, United States
[b] Michigan Technical University, 1400 Townsend Drive, Houghton, MI 49931, United States
[c] Alpha Star Corporation, 5199 East Pacific Coast Highway, Long Beach, CA 90804, United States

Received 13 January 2006; accepted 17 January 2006
Available online 17 April 2006

Abstract

A new, novel test method, associated analysis, and experimental procedures are developed to investigate the toughness of the facesheet-to-core interface of a sandwich material at cryogenic temperatures. The test method is designed to simulate the failure mode associated with facesheet debonding due to high levels of gas pressure in the honeycomb core. The effects of specimen orientation are considered, and the results of toughness measurements are presented. Comparisons are made between room and cryogenic test temperatures. It was determined that the test method is insensitive to specimen facesheet orientation and strain energy release rate increases with a decrease in the test temperature. A reasonable agreement between test and simulation was achieved at both temperatures.
Published by Elsevier Ltd.

Keywords: Sandwich material; Composites; C. Delamination; Cryogenic temperature; Launch vehicle

1. Introduction

Future space transportation vehicles will require lightweight structures and materials to meet the increased demands on performance. One area identified as a potential source for significant weight reduction is the replacement of metallic cryogenic fuel tanks with polymeric matrix composite (PMC) tanks. A promising structural concept based on PMC materials is to use a sandwich construction with the PMC as the facesheet material and lightweight polymeric honeycomb materials as the core. As outlined extensively by [1], the sandwich construction technique has many advantages over typical stiffened skin concepts, not the least of which is reduced weight. However, sandwich construction has a number of potential problems because the presence of multiple interfaces serves as a source for failure initiation and growth.

The interest in design of cryogenic-fuel tanks for spacecraft using polymeric composite materials goes back several years to the research associated with the National Aerospace Plane (NASP) and the single-stage-to-orbit (SSTO) vehicles [2]. Concepts were proposed for both the liquid-oxygen tanks and the liquid-hydrogen tanks. These studies addressed weight and cost benefits as well as the complex technical issues such as fatigue crack resistance and oxidation–corrosion resistance. It was recognized that permeation resistance of the tanks could be the overriding design criteria because of the implications that damage and the resulting permeation or leak would have on both durability and safety of the vehicle.

One of the first demonstrations of a PMC cryogenic fuel tank occurred in 1996 when the DC-XA suborbital demonstration vehicle was built with an all-composite liquid-hydrogen fuel tank [3]. The DC-XA tank was designed as an unlined and unstiffened cylinder measuring approximately 2.4 m in diameter. The tank performed as expected in both ground and flight tests.

* Corresponding author.
E-mail address: t.s.gates@larc.nasa.gov (T.S. Gates).

0266-3538/$ - see front matter. Published by Elsevier Ltd.
doi:10.1016/j.compscitech.2006.01.028

It was recognized that the unstiffened shell design would not work for larger tanks and would therefore require some other means to provide global and local stiffening. To avoid the potential weight penalties associated with a stiffened shell design, sandwich construction was considered. For an integrated cryogenic tank (i.e. one that is integral to the airframe structure), the tank wall must carry structural and pressure loads while operating over an extremely wide temperature range. One possible failure mechanism, associated with the use of sandwich materials in such a demanding environment, is debonding of the facesheet. This mechanism can occur due to high gas pressure inside the core material as a result of hydrogen leakage through the facesheet. This mechanism is facilitated by the occurrence of cryopumping. Cryopumping is a known phenomenon and is simply the condensation of a gas on a cryogenically cooled surface to produce a vacuum [4] that can occur during repeated cryogenic fluid fill and drain cycles. For a cryotank with PMC sandwich materials in the tank walls, this cryopumping will occur when the tank wall facesheet(s) develop leaks and allow the cryogen to permeate into the core. Subsequent warming of the cryogen causes a transition from a liquid to a gas phase and results in a substantial increase in core pressure. Without proper venting of this pressure, the core, facesheet, and bondline must sustain the resultant pressure-induced loads to prevent failure of the sandwich material [5]. The most likely initial failure mode due to cryopumping is facesheet-to-core debonding that can lead to crack growth and a total separation of the facesheet.

Most notably, this failure mode occurred in the NASA X-33 reusable flight demonstration vehicle. The X-33 was designed with a large ($8.7 \times 6.1 \times 4.3$ m), conformal tank made from a sandwich construction of polymeric composite skins and phenolic honeycomb core. After successful completion of the first protoflight pressure and loads test, the tank was drained of its liquid hydrogen fuel, and a purge of the tank began. Approximately 15 min after the tank was drained, the outer facesheet and core separated from the inner facesheet along part of the tank wall [6]. It was subsequently determined that many factors contributed to the tank failure however, considering the mechanics of the failure, it was found that the inner tank wall allowed permeation (and hence cryopumping) by way of microcracks in the facesheet. As pressure and strain decreased below that required to sustain the microcrack paths, the leak paths closed. As the tank warmed, the remaining trapped cryogens proceeded to vaporize, creating high pressure in the core. This pressure, coupled with bondline defects, likely caused the debond failure. The failure or debonding location occurred almost exclusively at the core-to-adhesive surface on the inner facesheet side.

The objective of this paper is to provide results on the combined experimental and analytical investigation of the facesheet-to-core debonding failure mode in PMC sandwich materials at cryogenic temperatures. The paper provides details on the material, test fixtures, test specimen design, test methods, model development, and fracture analysis. The experimental studies were performed at room temperature, −196 °C, and −269 °C to provide basic material properties and critical fracture parameters associated with failure. To obtain the fracture parameters, a novel test method was designed to simulate the failure mode associated with facesheet debonding in the presence of pressure in the sandwich core.

2. Material and test specimens

The test specimens were of a sandwich configuration made from an arrangement of composite facesheets, adhesive layers, metallic permeability barrier, and honeycomb core materials. This arrangement is shown schematically in Fig. 1. The test method was based on a three-point bend approach relying on the sandwich beam to react the bending load.

2.1. Materials

The PMC facesheet material used in this study was IM7/977-2 and the laminates consisted of a 15-ply quasi-orthotropic laminate ([45/90/−45/0/−45/90/45/0/45/90/−45/0/−45/90/45]) fabricated with a per-ply thickness of 0.132 mm. Fundamental lamina and laminate properties are given in Table 1 as a function of temperature. The core material was Kevlar 6.0pcf, 3/16" (non-perforated), the adhesive was EA9696AL, and the permeability barrier was 5056-H39 (3.5 mil) aluminum foil. All test panels used in this study were fabricated at the Northrop Grumman Corporation.

For reference purposes, the sandwich *longitudinal* direction was defined as the direction parallel to the core ribbon direction and the *transverse* direction was defined as the direction perpendicular to the ribbon direction (Fig. 2). The core material was manufactured in a regular hexagonal pattern and the average area of the core hexagon was estimated to be 24.2 mm^2. The *inner* facesheet was defined as the laminate to be debonded during tests and the *outer* facesheet was defined as the opposite laminate.

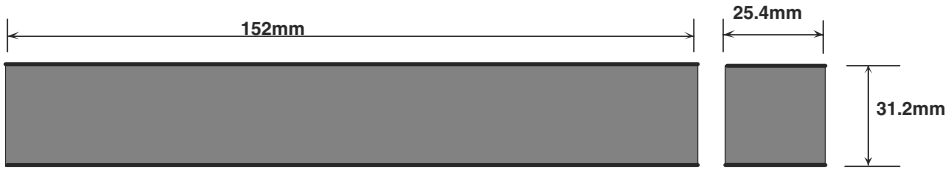

Fig. 1. Schematic of test specimen.

Table 1
Measured material properties of IM7/977-2 facesheets

	23 °C	−196 °C	−269 °C
E_1 (Gpa)	180.16	134.58	158.58
E_2 (Gpa)	8.27	11.38	11.58
G_{12} (Gpa)	6.21	7.17	7.79
α_{11} (mm/mm/°C)	−1.30	−1.49	−2.77
α_{22} (mm/mm/°C)	19.45	20.05	18.46
E_x (GPa)	60.47	49.23	56.14
E_y (GPa)	70.74	56.67	65.64
G_{xy} (GPa)	27.44	22.06	25.51

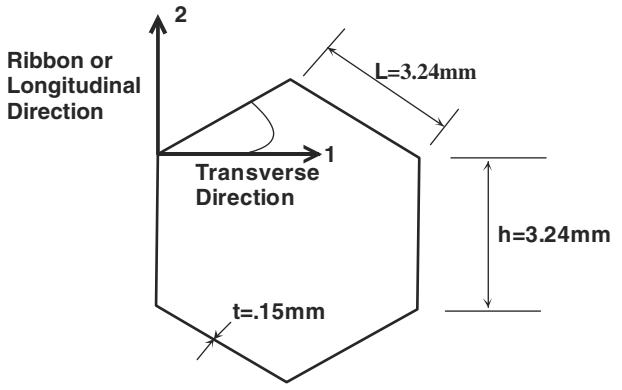

Fig. 2. Geometry of typical core cell.

Using the definitions provided by [1], the relative density of the core is calculated from

$$\frac{\rho^*}{\rho_s} = \frac{(\frac{t}{l})(\frac{h}{l}+2)}{2\cos\theta(\frac{h}{l}+\sin\theta)} \quad (1)$$

where ρ^* and ρ_s are the honeycomb-core density and density of core base material, respectively. As shown in Fig. 2, for the following dimensions:

$$\theta = 30^\circ, h = 3.86\text{ mm}, l = 2.67\text{ mm}, t = 0.15\text{ mm}$$

give a relative core density of 0.057. Defining the coordinate directions for the core to be ((1)–(3)) where (1,2) are in the plane of the hexagon (Fig. 1) and (3) is out of the plane, and using the superscript * and the subscript *s* to define the honeycomb and base material, respectively, expressions for directional modulus (E) are found in [1].

$$\frac{E_1^*}{E_s} = \frac{E_2^*}{E_s} = 2.3(t/l)^3 \quad (2)$$

Eq. (2) implies a very low relative stiffness of the core for in-plane loading. For out-of-plane loading, [1] provides the formula to estimate the relative, out-of-plane stiffness, that is,

$$\frac{E_3^*}{E_s} = \frac{\rho^*}{\rho_s} = 0.057 \quad (3)$$

2.2. Fracture test specimens

Fracture tests were conducted on rectangular beam specimens of the sandwich material. As shown in Fig. 1, the tests specimens were cut into a beam shape with the overall dimensions of $152 \times 25.4 \times 31.2$ mm. The intent of the fracture tests was to debond the inner facesheet by growing a crack along the core/adhesive/facesheet interface region. Figs. 3 and 4 illustrate the position of the specimen relative to the test fixture. To provide space for the center load bar, each test specimen had a 25.4 mm diameter through-hole cut in the specimen adjacent to the inner facesheet at the midpoint of the length. To facilitate the growth of the crack, a starter crack was cut across the width on each side of the hole with a thin saw blade to approximately one cell depth along the facesheet-to-core interface.

2.3. Push-off test fixture

As illustrated in Fig. 3 and the photograph of Fig. 4, a unique test fixture was developed [7] to perform the facesheet push-off fracture tests. The basic concept for this test was to use a three-point bend apparatus that loaded the facesheet from inside the sandwich beam and grew a crack along the interface region of the core, adhesive, and facesheet. The applied load was reacted at the ends of the beam by circular rods acting as simple supports. A stiff base plate supported the whole apparatus. For the cryogenic tests, the apparatus was placed in an aluminum vessel that was filled with liquid nitrogen or liquid helium prior to the start of the test run. As shown in the schematic of Fig. 3, the apparatus and test specimen remained submerged in the cryogenic fluid during the course of the test run.

3. Fracture analysis

Although the facesheet debond or fracture behavior of PMC sandwich materials at cryogenic temperatures has not been studied previously, the influence of temperature on the strain-energy release rate for laminated composite materials has been examined in recent studies. In one study [8], the tests were performed on an epoxy based composite material using the double cantilever beam (DCB) specimen. It was found that the value of strain-energy release rate (SERR), G (Mode I), increased approximately twofold when the test temperature was lowered from room temperature to −196 °C. In a similar study [9], it was found that the value of G (Mode I, DCB specimen) for the material IM7/977-3 decreased when the temperature was lowered from room temperature to −196 °C by a factor of approximately 1.50. These somewhat conflicting studies indicate that additional work may be required to standardize toughness tests at cryogenic temperatures for laminated materials.

For the sandwich materials, a debond forming near the skin–core interface can be of two types: interface and sub-interface. Interface cracks grow between the skin and core and sub-interface cracks form when an initial interface crack kinks into the core and then propagates parallel to the skin within the core. The type of delamination considered by the current work is limited to the interface type.

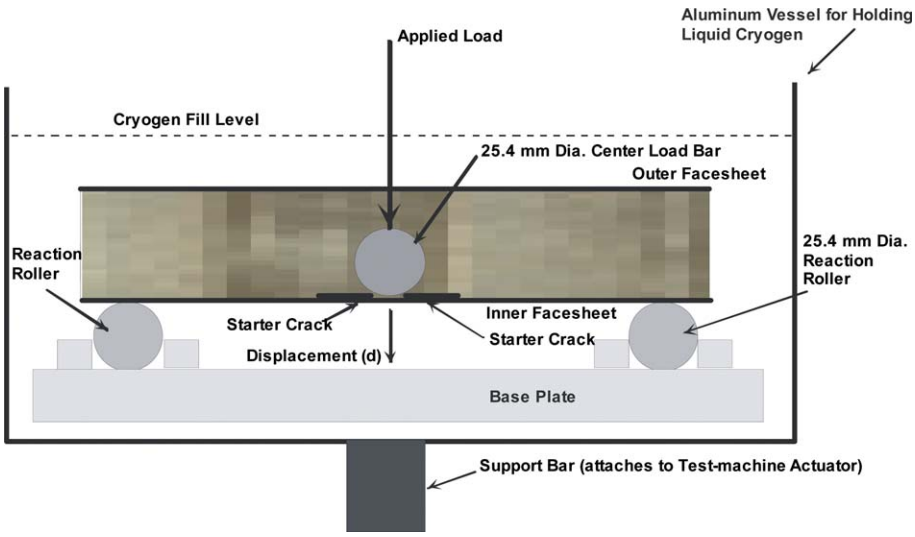

Fig. 3. Schematic illustration of test specimen, loading apparatus and cryogenic vessel.

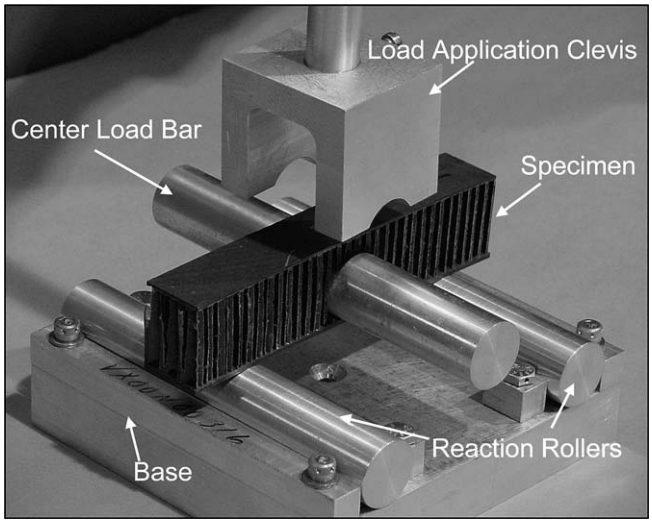

Fig. 4. Photograph of loading apparatus and test specimen.

Sun and Jih [10] examined the finite element-based numerical solution of SERR for interfacial cracks in bi-material media. They determined that the total SERR (G_T) remained constant, while the Mode-I (G_I) and Mode-II (G_{II}) SERRs converged to one-half G_T as the finite element size at the crack front was decreased. Further element mesh refinement then resulted in oscillating values for G_I and G_{II}. They concluded that an element size at the crack front on the order of 10% of the crack length resulted in relatively constant values for G_I and G_{II} and suggested that this be used for analysis.

The intent of the push-off test method used in this study was to simulate the fracture-induced failure mode by growing a crack in the core-to-facesheet interface region. Measuring the associated applied load and calculating the critical strain-energy release rate, or fracture energy as a function of crack length, allowed for the calculation of the fracture energy associated with the crack growth. Due to the loading and the relatively low shear stiffness of the core material, it was assumed that the fracture mode was predominately Mode I for this test.

The analysis method outlined here is based on the compliance calibration method, or Berry's method, as given by [11] and [12]. Additional information on this method and other types of Mode I fracture tests can be found in [13].

3.1. Compliance

The calculated compliance of the test specimen is based on the load and displacement measurements during test. The compliance is given by

$$C = \frac{P}{\delta} \tag{4}$$

where C is compliance, P is load and δ is the fixture displacement at the point of load application. Specimen compliance is then related to crack length through an empirical relationship,

$$C = ba^m \tag{5}$$

where a is the crack length, and b and m are empirical constants determined through a linear fit to a double logarithmic plot of C versus a.

3.2. Strain-energy release rate

In general, the critical SERR is a function of the strain energy and crack length

$$G_c = \frac{dU}{da} \tag{6}$$

where G_c is the critical SERR and U is the strain energy. For a specimen of width w, Eq. (6) gives

$$G_c = \frac{P\delta}{2wC}\frac{dC}{da} \tag{7}$$

and then using Eqs. (4) and (5), the critical SERR rate becomes

$$G_c = \frac{P^2}{2w}(mba^{(m-1)}) \tag{8}$$

From this last equation, the critical SERR is calculated by using the four experimentally determined parameters: m, b, a, and P.

3.3. Finite element analysis

Simulation of the interface debond failure was performed with a two-dimensional finite element analysis (FEA) using the commercial code GENOA (Alpah-Star Corporation). The paper will present details on the simulation methods and results from parametric studies on the predicted effects of load and temperature on failure.

Finite-element models were created for the given push-off test configuration. The model, illustrated in Fig. 5, was constructed with 2488 nodes and 2314 (8-node) shell elements. The load introduction apparatus provided minimal contact area with the test specimen therefore a concentrated load was utilized to represent the test load applied to the face sheet. It was assumed that the honeycomb core was not underneath the applied load during the loading process. The mode I type of failure of the interface, observed in the test, provided the basis for this assumption.

Fig. 6 shows the close-up of the pre-crack area in the model. This figure illustrates the degree of detail for the face sheet, honeycomb core and adhesive interface. Although comparative studies were not performed, based on previous experience with fracture analysis and the size of the crack relative to the surrounding constituents, the degree of mesh refinement in the vicinity of the crack tip was deemed suitable to model the local behavior. The test results demonstrated that the crack grew in the adhesive interface layer. The adhesive interface was modeled as 0.556 mm thick to represent a thin layer yet avoid the potential for numerical difficulties associated with extremely thin elements. For the same reason, the aluminum foil was not included in the model. The rationale for this was that since the delamination occurred in the interface on the core side and not in the thin aluminum foil, this modeling simplification would not influence the response or failure prediction of the model.

The facesheets were modeled as orthotropic with temperature dependency taken from Table 1 while the core was modeled as follows. The Young's moduli of the core were derived using Eqs. (2) and (3). The shear moduli and Poisson ratios were obtained using the formulas provided in [4].

$$G_{13} = G_{23} = 4t/3rG_s \tag{9}$$

$$G_{12} \approx 0 \tag{10}$$

Here, r represents the diameter of the inscribed circle in the hexagon cell. Poisson ratios were obtained by the following formulas.

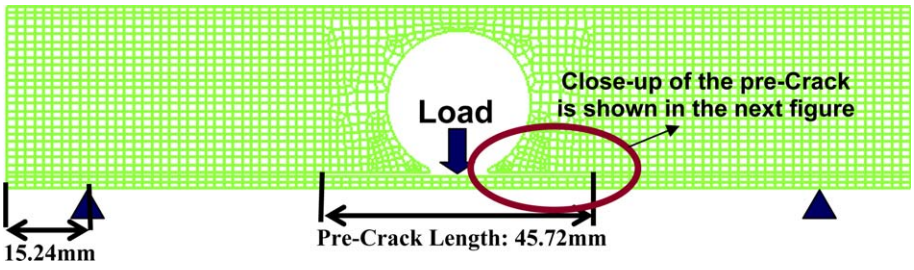

Fig. 5. Finite element model of test specimen.

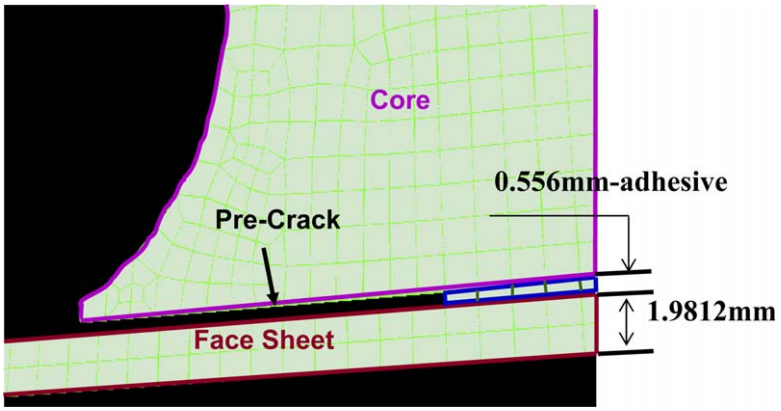

Fig. 6. Finite element model of pre-crack region.

$$\upsilon_{31} = \upsilon_{32} = \upsilon_s \quad (11)$$

$$\upsilon_{13} = \upsilon_{23} = 0 \quad (12)$$

$$\upsilon_{12} = 1 \quad (13)$$

As before, note that the subscripts 1 and 2 represent the in-plane two directions of the core. The subscription 3 is the out-of-plane direction of the core. The core material thickness and the edge length of the core cell are represented as t and l, respectively. The relevant core data are: Young's modulus 1515.68 GPa, shear modulus 96.50 GPa, Poisson's ratio 0.35. The properties at room and cryogenic temperatures were assumed the same in simulation.

The interfacial adhesive was assumed to behave as a typical epoxy material. The strength of the adhesive was not available, therefore, a strength value was obtained by noting the measured load deflection behavior of the sandwich and from that data establishing the pre-crack opening load to be 890 N for a pre-crack length of 45.7 mm. Due to the lack of experimental data, the same value of adhesive strength was used in the entire crack opening process at both room and cryogenic temperatures in the finite element simulation. Adhesive properties used in the simulation are: Young's moduls 3.48 GPa, Poisson's ration 0.35, strength 34.47 GPa.

It was assumed that the energy released due to fracture at the interface equaled the energy required to form the equivalent "new" surfaces. Fracture toughness is defined as the energy released per unit area. The finite element method calculates the entire deformation process during loading of the specimen, which includes every fracture event. In each fracture event, the corresponding crack length is determined and the released strain energy is computed using the relationships given in Eqs. (4)–(8) above. The in situ fracture toughness (critical strain energy release rate) can be derived based on the relationship between the released strain energy and the crack length at current fracture event. The simulation used displacement control.

4. Test plan

The laboratory test plan was constructed to investigate the fracture toughness as a function of two variables; that is, temperature and specimen orientation. The three test temperatures investigated were room temperature (23 °C) and two cryogenic temperatures (liquid N_2 at −196 °C and liquid/gaseous He at −253 °C). The two specimen orientations investigated were longitudinal and transverse, where the orientations were defined previously. At least three replicates for each test condition were used to develop the final data.

5. Experimental methods and procedures

The use of the novel test presented herein required development of new experimental methods and data-reduction procedures. The test methods fall into one of two broad categories; facesheet push-off and debond crack measurement.

5.1. Push-off test

The push-off test was run in a servo-hydraulic test machine using displacement control at a rate of 0.0254 mm per second. Load, as measured by the test machine load cell, and displacement, as measured by the test machine transducer, were monitored and recorded as a function of test time at a sampling frequency of 0.25 Hz.

By adjusting the starting position of the actuator, the initial applied load for each test was kept at zero. A typical test run had several distinct sections or events that are illustrated in the typical load-versus-displacement data of Fig. 7. During the loading phase of a test, the load-versus-displacement curve was approximately linear until the crack started to grow.

Due to the nature of the crack growth in the honeycomb/facesheet interface, the major portion of crack growth would occur with a significant and fast reduction in load. At this point in the test, the test operator would initiate a controlled reversal in displacement that would result in unloading of the test specimen.

The unloading phase had two distinct portions that were distinguished by an abrupt change in the slope of the load-versus-displacement curve. This abrupt change is also illustrated in Fig. 7. The compliance, as given by Eq. (4), was determined from this final unloading portion of the curve. The effective crack length, calculated using the procedures described below, was then plotted as a function of compliance on a double logarithmic scale and fit with Eq. (5) as illustrated by the example data presented in Fig. 8.

In general, the crack growth associated with such a test run would be small but measurable and would represent some fraction of the total specimen length. In order to quantify the crack length as a function of load and displacement, this typical test run would then be repeated 3–5 times or until the crack approached to within approximately 25 mm of the reaction rollers. Load

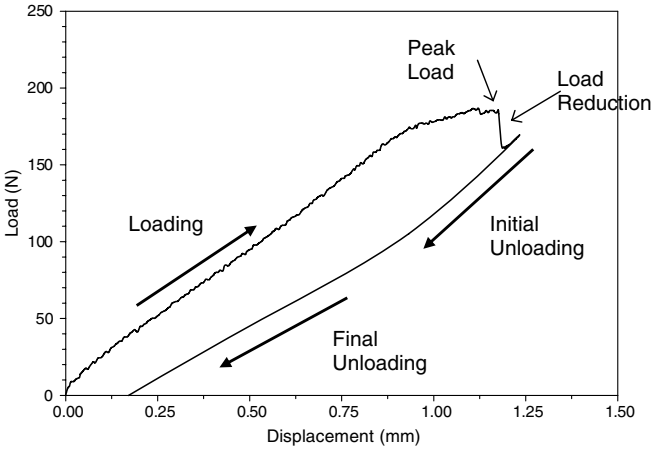

Fig. 7. Typical load-displacement curve illustrating each region of the test.

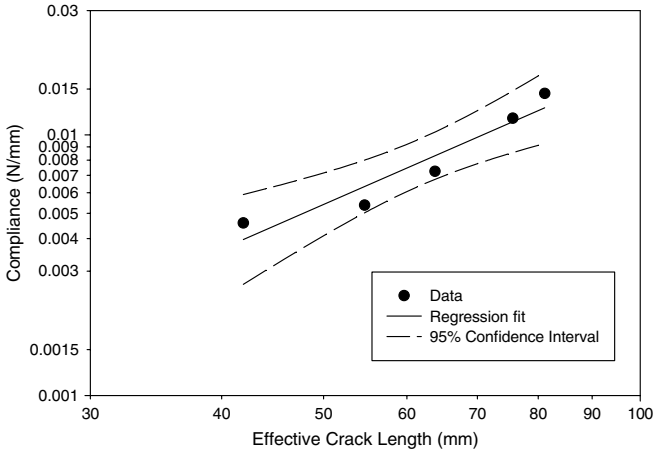

Fig. 8. Crack growth versus compliance data with linear fit.

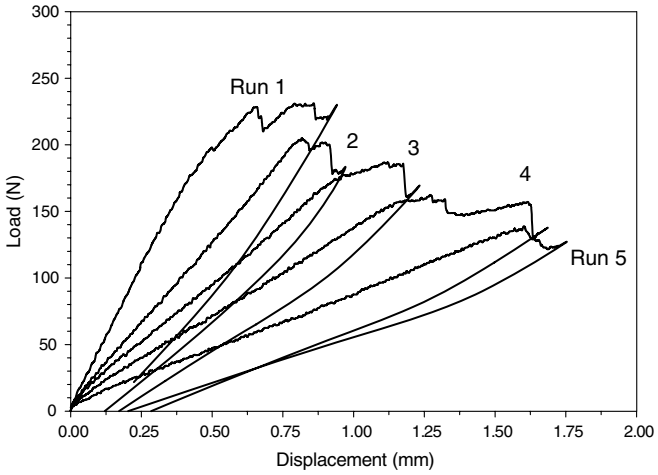

Fig. 9. Load–displacement data from a typical test sequence.

versus displacement data for a typical series of test runs is given in Fig. 9.

5.2. Crack measurement via X-ray inspection

The crack, which developed during the course of loading, was quantified by calculating an effective crack length based on the number of debonded cells. To quantify this debond, the specimen was removed from the test fixture after each run and examined by an X-ray radiography method. Briefly, this method consisted of injecting a small amount of dye penetrate into the crack on both sides of the center hole and then subjecting the specimen to a focused X-ray in the through-the-thickness direction. As shown by the typical X-ray images in Fig. 10, the debonded cells appeared as dark regions on the image and were easily distinguishable. As illustrated in Fig. 10, the center section of each specimen was where the cut-out was made to accommodate the load bar.

With an accurate count of debonded cells established, an effective crack length was then calculated using

$$\bar{a} = \frac{A_c n_{DB}}{w} \tag{14}$$

where $\bar{a}$ is the effective crack length, A_c is the area of a single cell (given previously), n_{DB} is the number of debonded cells counted in the X-ray image, and w is the specimen width. It should be noted that the cells in the center cut-out area and those cells debonded by the starter crack were also counted as debonded cells and used in calculating n_{DB}.

After completion of all the test runs, the inner facesheet was completely separated from the remaining bonded core and the failure surface was examined visually.

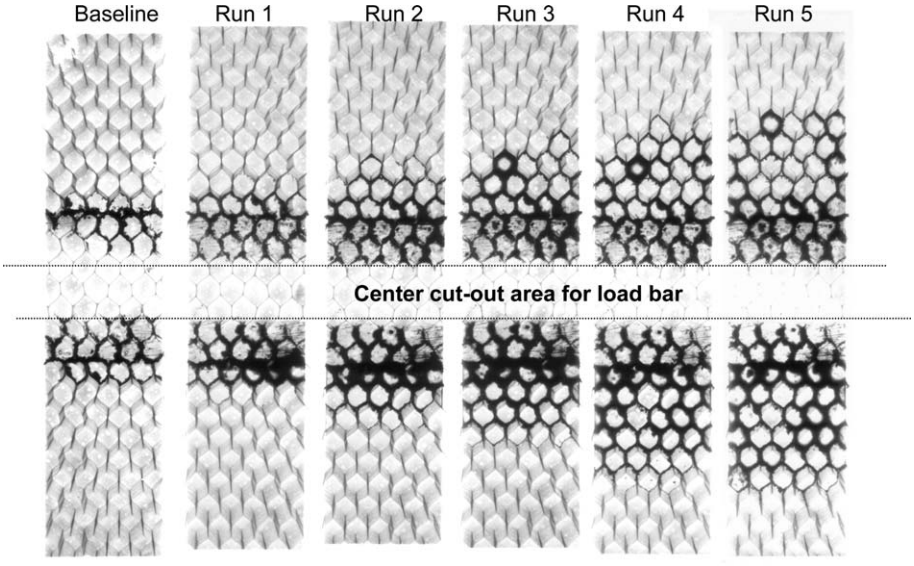

Fig. 10. Through-thickness X-ray of sandwich specimen showing growth of delaminated region (darkened cells).

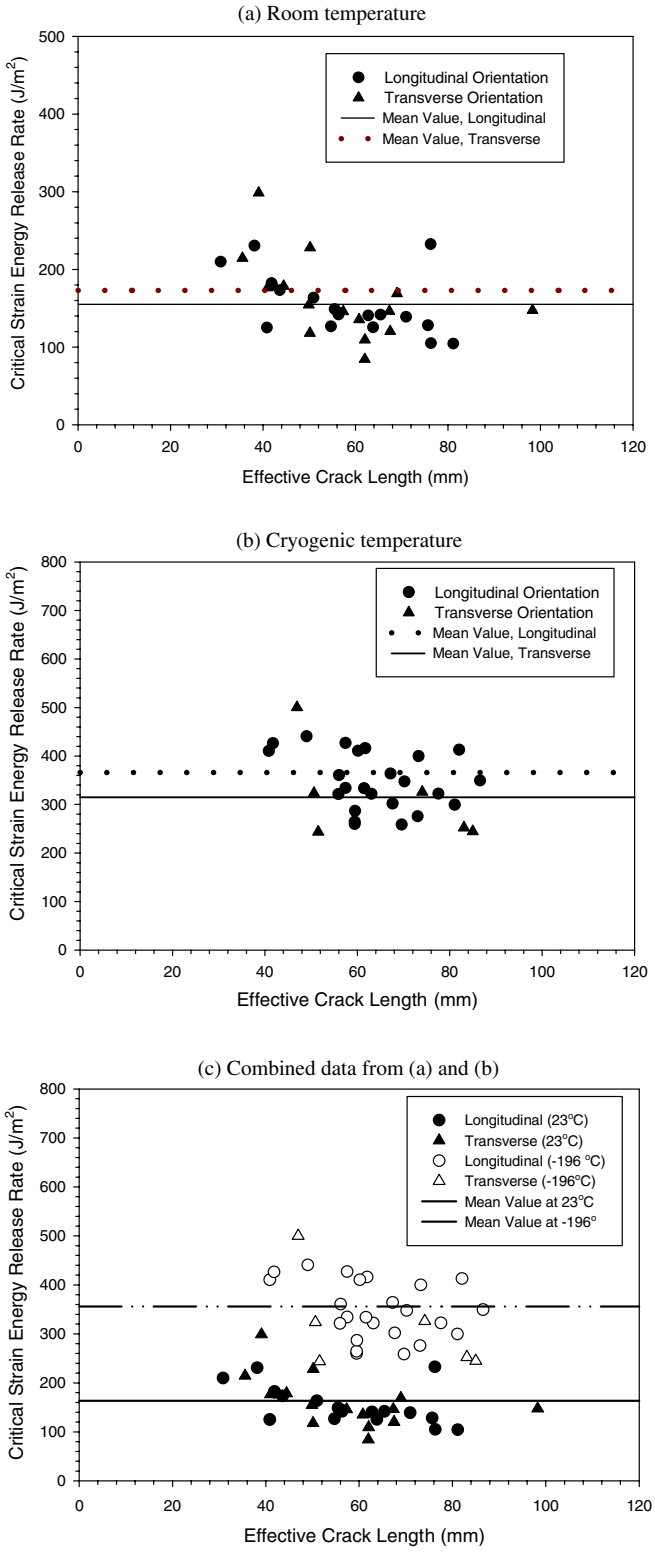

Fig. 11. Toughness data from both directions at room and cryogenic temperatures.

6. Results

The primary variables considered in this study were specimen orientation (transverse versus longitudinal) and test temperature. The impact of these variables on specimen stiffness, strain-energy release rate, crack growth, and the fracture surface will be considered herein.

6.1. Material stiffness

Review of the data in Table 1 clearly indicates that the facesheet stiffness was a function of both orientation and temperature. Orientation was the biggest factor with a difference in stiffness between longitudinal and transverse directions on the order of 15%. Both facesheets, regardless of orientation, exhibited a small decrease in stiffness with a decrease in temperature.

In comparison to many commercial systems [1] that can have relative densities in the range of 0.2–0.3, the relative density (Eq. (1)) of the core was quite low. Correspondingly, the in-plane and out-of-plane stiffness, as given by Eqs. (2) and (3), respectively, were also low, compared to many commercial systems.

6.2. Measured strain-energy release rate

The critical SERR G_c (Eq. (8)) was found for all test temperatures. In order to characterize the critical SERR, mean values were computed by using all the data over the entire range of effective crack length. Fig. 11 provides the computed values of strain energy release rate for a given effective crack length.

The room temperature data indicates that there was no appreciable scatter between the replicate specimens. In general, G_c tended to decrease as crack length increased. Comparison of longitudinal and transverse direction data at a given temperature indicates that there is no appreciable dif-

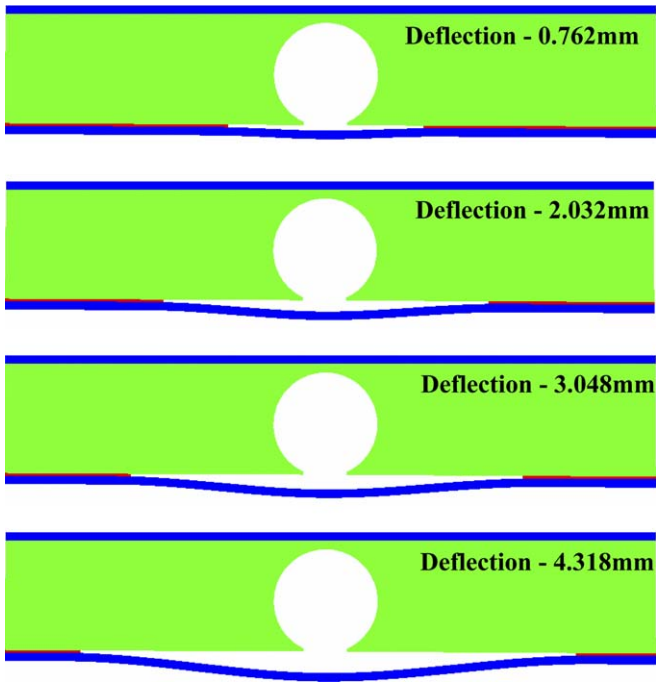

Fig. 12. Deformation and fracture process for the FEM.

ference between the mean values of the longitudinal and transverse data. Therefore, these data sets were combined at each temperature.

The lack of significant differences between G_c for the −196 °C and −269 °C tests prompted the combination of these data sets into a single "cryogenic temperature" data set. As with the room temperature data, the cryogenic temperature data showed some decrease with increasing crack length. The mean value of the cryogenic G_c is greater than the room temperature value and the degree of scatter increased as compared to the room temperature data. Data scatter was attributed to the increased difficulty in discerning distinct crack growth while enclosed in the cryogenic test chamber as compared to the ease of operation at room temperature. Both data sets were combined into one plot, Fig. 11, to illustrate the overall toughness trend with temperature. The mean values of G_c, were computed and it was determined that G_c increased by approximately 20% with a decrease from room to cryogenic temperatures.

6.3. Crack growth and the fracture surface

The X-ray images for most specimens showed relatively stable crack growth as a function of the load. However, in some cases the crack front was not uniform and the debonded region was irregular. In all cases, Eq. (9) was used to calculate the effective crack length.

For all cases, regardless of test temperature, the post-test examination of the fracture surface showed that failure always occurred along the core-to-adhesive bond line. The core separated cleanly from the inner barrier film and the adhesive tended to remain bonded to the inner facesheet.

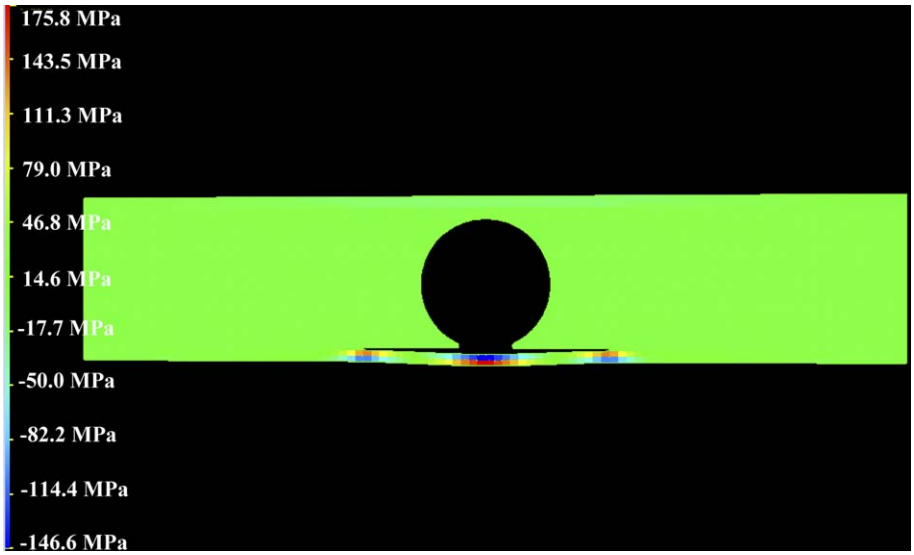

Fig. 13. Stress distribution in horizontal direction at room temperature.

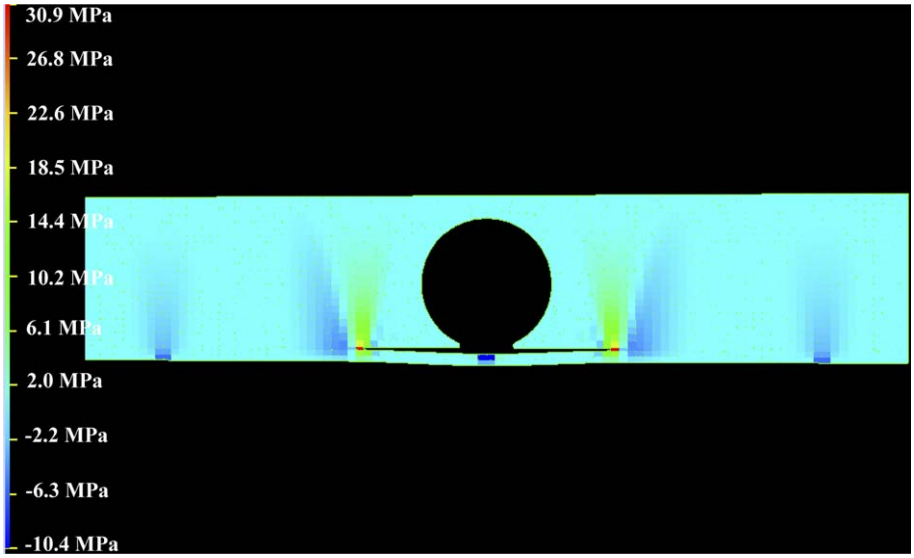

Fig. 14. Stress distribution in vertical direction at room temperature.

6.4. Finite element simulations

The deformation and fracture process is shown in Fig. 12. Only the simulation at room temperature is given here because the simulation at cryogenic temperature has the same pattern. The thin red layer is the adhesive interface. The two blue layers are the face sheets. The green block is the honeycomb core. The adhesive interface between the top face sheet and core was not modeled for simplifying the simulations. It can be seen that the crack propagated solely in the adhesive interface. Since the crack uniformly opened up and there was no twist or contortion occurring, it is reasonable to say that the fracture is of Mode I.

Stress distributions in the specimen at room temperature are illustrated at horizontal and vertical directions in Figs. 13 and 14, respectively. Fig. 15 shows the distribution of shear stress. In the three figures, the deflection of the face sheet is 0.762 mm. The stresses are mostly concentrated in the crack area. The stress levels in the other areas are relatively small.

Stress distributions in the specimen at cryogenic temperature are illustrated at horizontal and vertical directions in Figs. 16 and 17. Fig. 18 shows the distribution of shear stress. In the three figures, the deflection of the face sheet is 0.762 mm. Similar to the stress distributions at room temperature; the stresses at cryogenic temperature are mostly concentrated in the crack area. The stress levels in

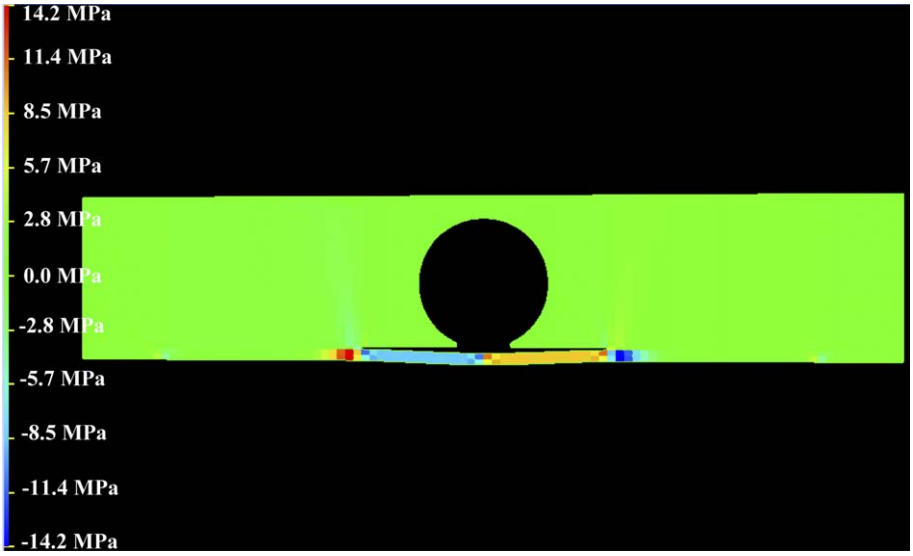

Fig. 15. Shear stress distribution at room temperature.

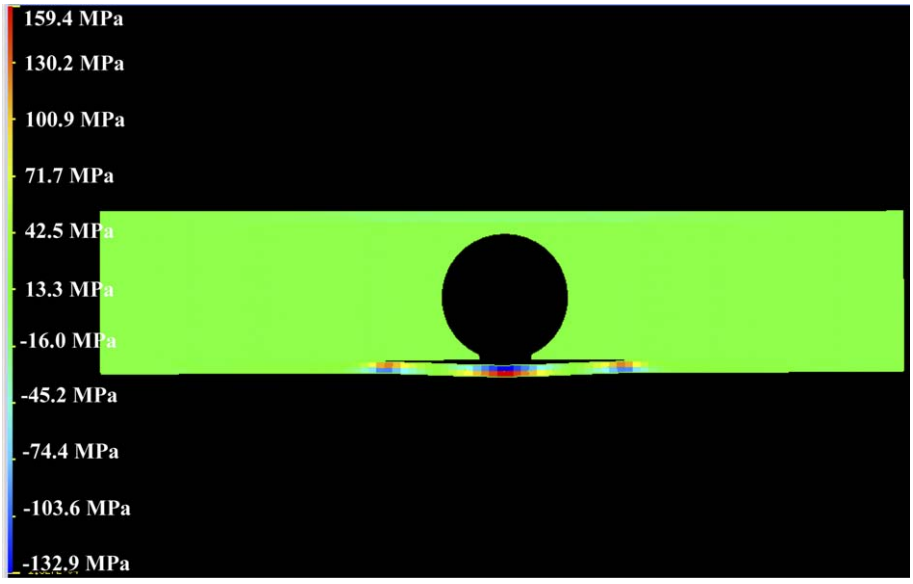

Fig. 16. Stress distribution in horizontal direction at cryogenic temperature.

the rest areas are relatively small. Compared with the case at room temperature, the stress levels at cryogenic temperature are smaller.

The simulation utilized displacement control. The load–deflection relations of the specimen at room and cryogenic temperatures are shown in Fig. 19. Each vertical drop on the curves represents a fracture event, which was caused by the stress relief due to fracture. The overall trend of the load–deflection curves is downward after the first occurrence as the specimen continued losing stiffness at each fracture event.

The relationships between the specimen compliance and crack length are illustrated in Fig. 20 for room and cryogenic temperatures, respectively. Each curve was fit using the power law function, which gives the constant b and exponent m in Eq. (12). The specimen compliance increased as the crack propagated. The compliance at cryogenic temperature increased faster than that at room temperature, which is reflected by the bigger b and m at cryogenic temperature.

Based on the Eqs. (8)–(12) and parameters, m,b,a, and P, determined in Fig. 20, the fracture toughness of the adhesive interface can be derived in the form of the critical strain energy release rate. The simulation results as well as the test data are illustrated in Fig. 21 for both room and cryogenic temperatures.

The simulations show the critical strain energy release rates increased a little in the initial propagation of the crack, and then quickly became stabilized. This indicates the released strain energy per area kept constant during

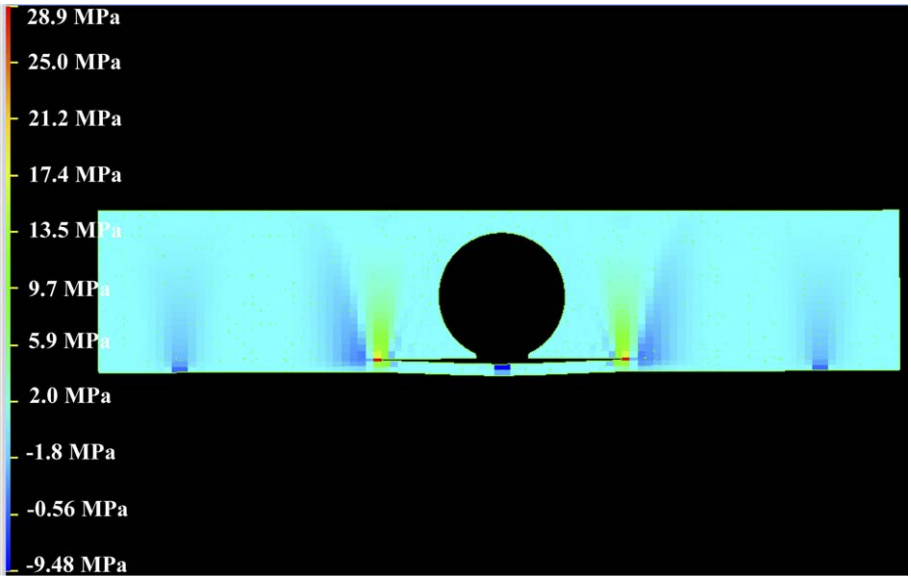

Fig. 17. Stress distribution in the vertical direction at cryogenic temperature.

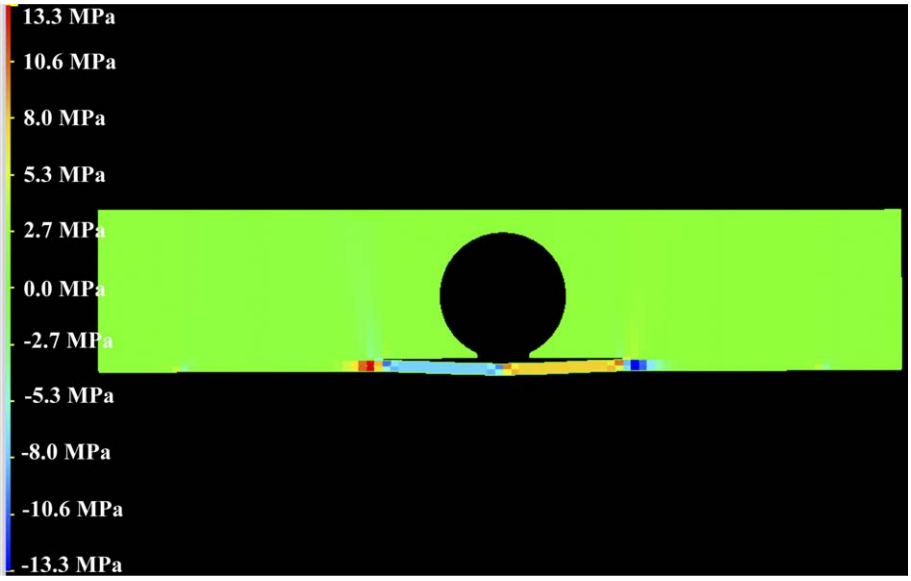

Fig. 18. Shear stress distribution at cryogenic temperature.

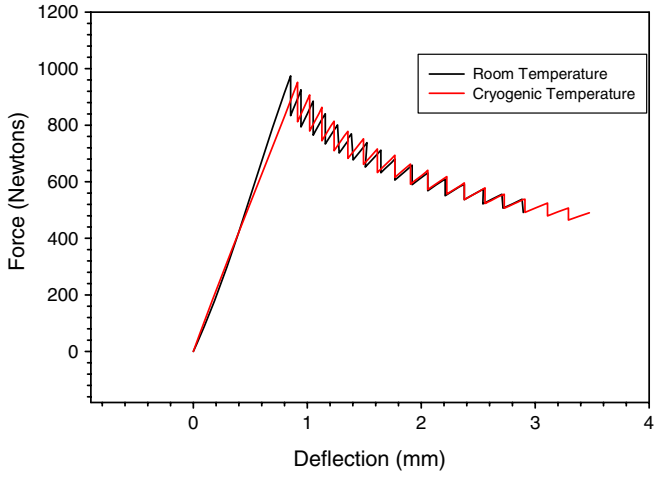

Fig. 19. Computed load versus deflection at each temperature. Each vertical drop represents a fracture event.

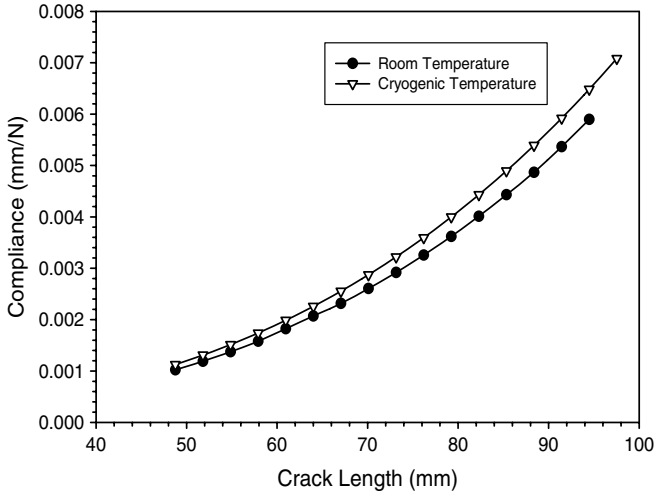

Fig. 20. Computed compliance versus crack length at each temperature.

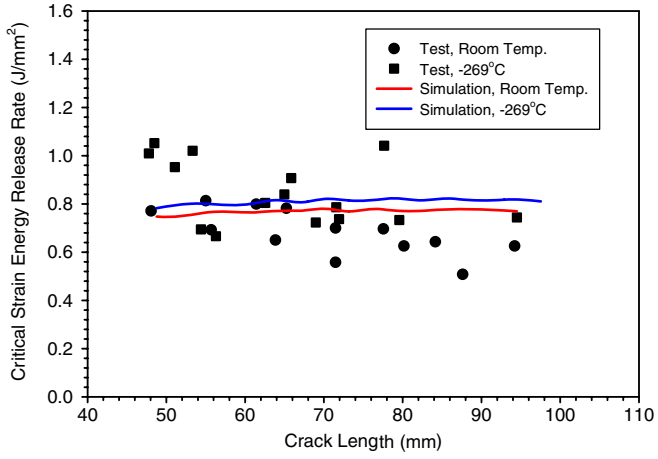

Fig. 21. Comparison of simulated and measured toughness data at both temperatures.

the fracture process. Therefore, the fracture toughness is independent of the crack length as the simulations show. However, test data indicates a decrease of the fracture toughness as the crack grew. Considering the scattering in test data, a constant value of the fracture toughness may be assumed with reasonable accuracy.

Both the simulation and test results show the toughness of the adhesive interface became higher at cryogenic temperature compared to that at room temperature. The only input difference between the simulations at the two temperatures was the face sheet stiffness.

7. Summary and concluding remarks

The in-plane stiffness of the composite facesheets was dependent on specimen orientation and test temperature. In general, the stiffness of the facesheets increased with a decrease in temperature. Therefore, it is expected that the bending stiffness of the entire test specimen would be a function of facesheet orientation and exhibit an increase as test temperature decreases.

Examining the SERR results from the current study of sandwich material, it was determined that G_c was independent of sandwich specimen orientation regardless of test temperature. It is significant, however, that G_c increased with a decrease in temperature. In general, the G_c data was insensitive to changes in crack length. Finite element simulation of the fracture process reasonably agreed with the measured response taking into account the scatter of the measured data. Additional refinement of the local mesh and a more complete set of temperature dependent material properties of the core and adhesive may be required to provide an improvement in agreement best test and simulation.

The test apparatus and associated experimental methods developed in this study provide a novel approach to measuring the toughness of the facesheet-to-core bond and simulating the loading due to internal, core pressure. The primary experimental difficulties associated with this test method are related to the measurement of crack length. Further development of experimental techniques may lead to a more precise, in situ means of crack-growth measurement for a specimen immersed in cryogenic fluid.

References

[1] Gibson LJ, Ashby MF. Cellular Solids, Structure and Properties. Cambridge Solid State Science Series. Cambridge: Cambridge University Press; 1997.

[2] Robinson MJ. Composite cryogenic propellant tank development. In: Proceedings of the 35th structures, structural dynamics, and materials conference. AIAA-94-1375-CP. South Carolina: Hilton Head; 1994.

[3] Robinson MJ. Composite structures on the DC-XA reusable launch vehicle. In: Proceedings of the 28th international SAMPE. Seattle, Washington; 1996.

[4] Barron RF. Cryogenic systems. 2nd ed. New York: Oxford University Press; 1985.

[5] Robinson MJ, Eichinger JD, Johnson SE. Hydrogen permeability requirements and testing for reusable launch vehicle Tanks. In:

Proceedings of the 43rd AIAA/ASME/ASCE/AHS structures, structural dynamics, and material conference. AIAA-2002-1418. Denver, Colorado; 2002.

[6] NASA, Final report of the X-33 liquid hydrogen tank test investigation team. George C. Marshall Space Flight Center, NASA Report; May 2000.

[7] Gates TS, Herring HM. Facesheet push-off tests to determine composite sandwich toughness at cryogenic temperatures. In: Proceedings of the AIAA 42nd SDM conference. AIAA-2001-1219. Seattle, WA; 2001.

[8] Aoki T et al. Mechanical performance of CF/polymer composite laminates under cryogenic conditions. In: Proceedings of the 41st structures, structural dynamics, and materials conference. AIAA-2000-1605. Atlanta (GA): American Institute of Aeronautics and Astronautics; 2000.

[9] Donaldson SL, Kim RY. Interlaminar fracture of carbon fiber reinforced epoxy and bismaleimide composites at cryogenic temperatures. In: American Society of Composites, 15th Technical Meeting2000. College Station (TX): American Society of Composites; 2000.

[10] Sun CT, Jih CJ. On strain energy release rates for interfacial cracks in bi-material media. Eng Fract Mech 1987;28(1):13–20.

[11] Berry JP. Determination of fracture energies by the cleavage technique. J Appl Phys 1963;34(1):62–8.

[12] Cantwell WF, Davies P. A test technique for assessing core–skin adhesion in composite sandwich structures. J Mater Sci Lett 1994;13:203–5.

[13] O'Brien TK, Martin RH. Round robin testing for mode i interlaminar fracture toughness of composite materials. J Compos Technol Res 1993;15(4):269–81.